Journal of Molecular Spectroscopy **216,** 1–14 (2002)
doi:10.1006/jmsp.2002.8669

Photoelectron Spectroscopy of Nickel, Palladium, and Platinum Oxide Anions

Tanya M. Ramond, Gustavo E. Davico,[1] Fredrik Hellberg, Fredrik Svedberg, Peter Salén, Patrick Söderqvist, and W. Carl Lineberger[2]

JILA, University of Colorado and National Institute of Standards and Technology, and Department of Chemistry and Biochemistry, University of Colorado, Boulder, Colorado 80309-0440

Received September 18, 2001; in revised form July 23, 2002

The 364-nm negative ion photoelectron spectra of XO and OXO molecules (X = Ni, Pd, and Pt) are reported. The spectra yield the electron affinities (EAs): $EA(\mathrm{NiO}) = 1.455 \pm 0.005$ eV; $EA(\mathrm{PdO}) = 1.672 \pm 0.005$ eV; $EA(\mathrm{PtO}) = 2.172 \pm 0.005$ eV; $EA(\mathrm{ONiO}) = 3.043 \pm 0.005$ eV; $EA(\mathrm{OPdO}) = 3.086 \pm 0.005$ eV; $EA(\mathrm{OPtO}) = 2.677 \pm 0.005$ eV. In addition, for the diatomics, transitions from the anion $\tilde{X}\,^2\Pi_{3/2}$ and $\tilde{X}'\,^2\Pi_{1/2}$ states into neutral $\tilde{X}\,^3\Sigma^-$, $^3\Pi$, and for NiO and PdO, $^1\Pi$, are assigned. Several states have been reassigned from those in the existing literature. Anion $^2\Pi_{3/2}$–$^2\Pi_{1/2}$ spin–orbit splittings are measured, as are neutral $^3\Pi_2$–$^3\Pi_1$ spin–orbit splittings: the XO $^3\Pi_2$–$^3\Pi_1$ splittings increase from 405 ± 30 cm^{-1} (NiO) to 805 ± 30 cm^{-1} (PdO) to 3580 ± 40 cm^{-1} (PtO). A bond length shortening of 0.03 ± 0.01 Å is measured upon electron detachment from NiO^-, resulting in an anion bond length of 1.66 ± 0.01 Å. The bond length does not change upon electron detachment from PdO^- using 3.4-eV photons. The Pt–O bond length decreases by 0.035 ± 0.010 Å in the $^3\Pi_1 \leftarrow {}^2\Pi_{3/2}$ transition. The spectrum of OPtO displays a significantly more extended vibrational progression than those of ONiO or OPdO, and the O–Pt bond length is found to decrease by 0.07 ± 0.01 Å upon electron detachment. The spectra support the view that the Ni–O bond is largely ionic, the Pd–O bond is somewhat less so, and the Pt–O bond displays a substantial covalent character.

Key Words: transition–metal oxides; electronic structure; negative ion spectroscopy; electron affinity; NiO; PdO; PtO; ONiO; OPdO; OPtO.

1. INTRODUCTION

Metal oxides play a central role in a variety of fields including high-temperature materials, catalysis, semiconductors, and electrode materials (*1–8*). Understanding their properties has both technological and fundamental importance. Despite this importance, relatively little information exists about the basic structure and properties of Ni, Pd, and Pt metal oxides, with the majority of the literature concentrating on the lighter metal oxides. The open *d*, *p*, and *s* shells give rise to enormous complexity in the energy level structure that provides a daunting challenge to theorists and experimentalists alike.

Spectroscopic studies (*9–16*) have identified the NiO $^3\Sigma^-$ ground state, measured the vibrational frequency, and obtained the electron affinity (*15, 16*). Friedman-Hill and Field (*11*) have provided a thorough characterization of the Σ^- ground state, a $^3\Sigma^-$ state at 16 000 cm^{-1}, and a $^3\Pi_i$ state at 4300 cm^{-1}. An essentially Ni^+O^- ionic picture of the NiO ground state has emerged (*11, 17*). The experimental work has been supported by various theoretical studies of NiO ground and excited electronic states (*17–23*).

Much less is known about PdO and PdO^-. Several theoretical investigations (*17, 24–30*) have concluded that either $^3\Sigma^-$ or $^3\Pi$ is the PdO ground state, both lying close in energy. Other theoretical studies have evaluated relativistic effects for PdO and PtO (*27, 30*). PdO is calculated to be quite ionic (*17*), although covalent bonds are formed. Jarrold has recently reported the photoelectron spectrum of PdO^- (*31*).

For PtO, more spectroscopic data are available than for PdO, although there are no anion photoelectron spectra. The electronic ground state of PtO was reported to be $^1\Sigma^+$ in early spectroscopic studies (*32–34*). Later, it became clear that the ground state is a $^3\Sigma^-$ state with a related low-lying state only 936 cm^{-1} above the ground state (*35*). Several investigators have (*32–34, 36*) reported transitions to visible and ultraviolet states of gaseous PtO, but there are very few data (*35, 37*) on those states lying lower in energy, 0–2 eV above the ground state. Theoretical efforts (*27, 38*) have primarily focused on relativistic effects on the molecular geometry and other physical properties.

Information on the metal dioxide species ONiO, OPdO, and OPtO is fragmentary. Experimental data exist for ONiO and OPtO (*14, 15, 39*), and a few theoretical studies have calculated molecular structures and electronic properties (*26, 29, 40*). Several photoelectron spectroscopic studies have been carried out on similar metal molecules, including CuO^- (*41, 42*),

[1] Present address: Department of Chemistry, University of Idaho, P.O. Box 2343, Moscow, Idaho 83844.

[2] To whom correspondence should be addressed. Fax: (303) 492 8994. E-mail: wcl@jila.colorado.edu.

0022-2852/02 $35.00

RhO^- (*43*), PdC_2H^- and PdC_2HN^- (*44*), and $PdCO^-$ and $PdCN^-$ (*45*).

A major complication associated with analysis of these metal oxide species arises from the failure of a single-configuration view of the metal oxide to provide a useful zero-order picture of the electronic state (*46*). The valence configurations of the metal oxides include open *s*-, *p*-, and *d*-shells, with molecular orbital energy orderings that depend on the electronic state and net charge. Furthermore, strong state mixing results in spectroscopic properties that bear little resemblance to any simple zero-order picture. All these reasons render theoretical calculations difficult, even without the additional complication of relativistic effects, including, most notably, the radial contraction of the *s* and *p* electrons along with the radial expansion of the outer *d* electrons, as well as spin–orbit splitting (*47*). The magnitude of these effects scales as Z^2 and becomes a major consideration for the sixth row metal oxides.

We report the 364-nm photoelectron spectra of several XO^- and OXO^- anions (X = Ni, Pd, and Pt). The electron affinities (*EA*s) for all six molecules are identified, as well as vibrational frequencies and bond length changes. Several low-lying electronic states of the neutral and anion XO molecules are assigned, allowing measurements of anion and neutral spin–orbit splittings. While the assignments reported here differ from some of the earlier photoelectron findings, the differences arise primarily from the better energy resolution available in the present apparatus. Vibrational frequencies for the OXO molecules are measured, as well as bond length changes upon electron detachment. The measurements obtained here provide a much improved, although still incomplete, description of the low-lying states of these oxides.

2. EXPERIMENT

As details of the negative ion photoelectron spectrometer and the general experimental procedure have been described previously (*48, 49*), only a brief overview is given here. The anions are synthesized in a flowing afterglow apparatus by the use of a cold cathode sputtering discharge, described in detail previously (*50, 51*). Briefly, it operates by sputtering clusters from a metal cathode with a DC discharge in a flowing afterglow source with a mixture of 10–15% argon in 0.5-Torr helium buffer gas. Metal cluster ions are produced when Ar^+ is accelerated toward the negatively biased (−2-kV) cathode that is made of a high purity Ni, Pd, or Pt rod, 5 cm long by 2 mm diameter. The cathode potential is typically about −1500 V with respect to the grounded flow tube. Metal oxide ions are produced by adding a trace of oxygen to the flow tube. Ion beam currents ranged from 80 pA for PtO^- to <10 pA for NiO^-. The anions produced in the sputter source are partially thermalized in collisions with the He buffer gas in the flow tube. However, spectra were also obtained with the flow tube cooled by liquid-nitrogen, substantially lowering the anion vibrational temperature. In this way, spectra were collected at both 300 K (no cooling) and 200 K (liquid-nitrogen-cooled) flow tube temperatures. In this paper, spectra obtained at these two flow tube temperatures will be referred to as warm and cold spectra, respectively.

Upon extraction from the flowing afterglow reactor, ions are mass-selected by a Wien velocity filter. The mass-selected beam is crossed with 100 W of 364-nm radiation from an argon ion laser in a build-up cavity. Photoelectrons ejected into a small solid angle perpendicular to the ion and laser beam plane are extracted into a hemispherical energy analyzer and detected by a position-sensitive detector, giving an overall energy resolution of ≈9 meV. Spectra are recorded in electron kinetic energy (eKE), which is related to the binding energy (eBE) via the laser photon energy: $eBE = h\nu - eKE$. The absolute energy scale is calibrated by the position of the $^3P_2 \leftarrow {}^2P_{3/2}$ transition in the O^- spectrum (*52*). A small energy scale compression factor (∼1%) is obtained from the positions of several well-known transitions in the W^- photoelectron spectrum (*53*). A half-wave plate is placed in the laser beam path just prior to entry into the build-up cavity. It is used to rotate the polarization plane of the laser to obtain photoelectron angular distributions and thus measure the anisotropy parameter β (*49, 54*). A harmonic-oscillator Franck–Condon program was used to simulate the vibrational progressions in the photoelectron spectra (*55*). Vibrational frequencies, origin peak position, and geometry differences between anion and neutral are directly determined from this simulation, without recourse to *ab initio* calculations.

3. ANALYSIS OF NiO, PdO, AND PtO

NiO

An orbital diagram of the ground state of NiO is presented in Fig. 1. Although it is an oversimplification and should not be interpreted too literally (*46*), it does provide a zero-order picture of the molecular orbitals to aid in analysis of the NiO^- photoelectron spectrum. The valence molecular orbitals are formed from the 3*d* and 4*s* orbitals of Ni combined with the 2*p* orbitals of O. The result is bonding 1σ and 1π orbitals, nonbonding

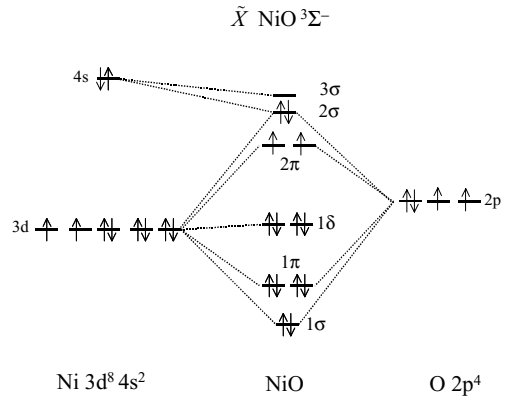

FIG. 1. Molecular orbital diagram of the $^3\Sigma^-$ ground state of NiO showing the mixing of atomic O and Ni orbitals.

1δ orbitals, and weakly antibonding 2π and 2σ orbitals. There are nonbonding 3σ orbitals formed primarily from the valence $4s$ orbitals of Ni, and the 3σ orbitals lie close to and mix with the 2σ orbitals. The ground state of NiO is a $^3\Sigma^-$ state best described as a $1\sigma^2 1\pi^4 1\delta^4 2\pi^2 2\sigma^2$ configuration (*9–11, 17–20, 56*) with substantial ionic character. To form NiO^-, the extra electron occupies one of the antibonding 2π orbitals, forming a $\pi^3\sigma^2\ ^2\Pi_{3/2}$ state. In the 3.408-eV photoelectron spectrum of NiO^-, we expect to observe several low-lying neutral NiO states through detachment of any one of the electrons in the 1δ, 2π, or 2σ orbitals. In general, detachment of an electron from an orbital with substantial $4s$ character is expected to produce intense photoelectron peaks due to the fact that their diffuse spatial distributions yield a large cross-section for detachment. However, because the 2σ and 3σ orbitals are expected to be close in energy, they can mix and it is not unreasonable in these molecules to expect intense $d\sigma$ electron detachment as well.

The 364-nm cold photoelectron spectrum of NiO^- taken with the laser polarized parallel to the photoelectron collection direction (0°) is displayed in Fig. 2. The spectrum shows many sharply resolved features, labeled A through W, with a large variation in intensity. All the peaks in the photoelectron spectrum exhibit angular distributions peaked along the laser polarization direction ($\beta > 1$) with the exception of peaks I and Q, which have an isotropic angular distribution, i.e., $\beta = 0$.

There have been two recent photoelectron spectroscopy studies of NiO^-, one by Wu and Wang (*15*) and one by Moravec and Jarrold (*16*). Both studies employed pulsed laser ablation ion sources coupled with time-of-flight electron kinetic energy analysis. The energy resolution varies between roughly 10 and 50 meV. For these metal oxides, this resolution results in blending several peaks together, masking many of the features observed here, changing their appearance or relative intensities. The consequence was that a full assignment of their spectra was quite difficult. The spectra reported here are generally consistent with the earlier data (*15, 16*), but the higher resolution permits observation of many new features that necessitate alternative interpretations. The differences in assignments are discussed below.

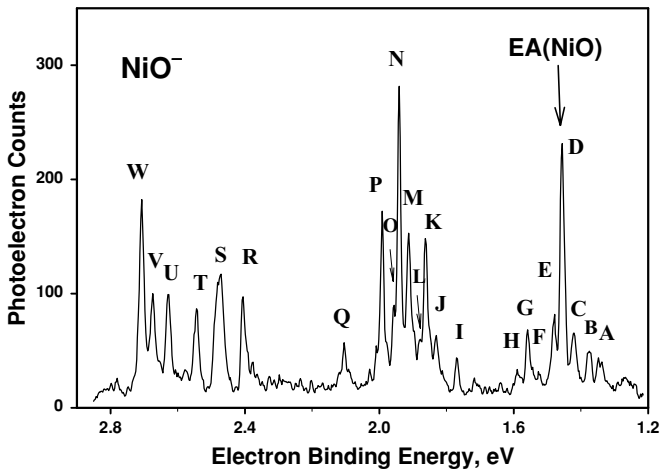

FIG. 2. 364-nm photoelectron spectrum of NiO^- taken at laser polarization angle 0° and flow tube temperature 200 K.

TABLE 1
Absolute and Relative Position and Assignments for Peaks in the Photoelectron Spectrum of NiO^-

Peak	Binding Energy, (eV)	Relative Position (cm^{-1})	Assignment
A		-910 ± 40	$\tilde{X}\,^3\Sigma^- \leftarrow \tilde{A}'$
B		-650 ± 30	$\tilde{X}\,^3\Sigma^- \leftarrow \tilde{A}$
C		-275 ± 30	$\tilde{X}\,^3\Sigma^- \leftarrow \tilde{X}'\,^2\Pi_{1/2}$
D	1.455 ± 0.005	0	$\tilde{X}\,^3\Sigma^-(v=0) \leftarrow \tilde{X}\,^2\Pi_{3/2}$
E		190 ± 35	$\tilde{X}\,^3\Sigma^-(v=1) \leftarrow \tilde{A}$
F		550 ± 40	$\tilde{X}\,^3\Sigma^-(v=1) \leftarrow \tilde{X}'\,^2\Pi_{1/2}$
G		825 ± 30	$\tilde{X}\,^3\Sigma^-(v=1) \leftarrow \tilde{X}\,^2\Pi_{3/2}$
H		1055 ± 40	$\tilde{X}\,^3\Sigma^-(v=2) \leftarrow \tilde{A}$
I	1.768 ± 0.005	0	—
J		-885 ± 30	$^3\Pi_2 \leftarrow \tilde{A}'$
K		-635 ± 30	$^3\Pi_2 \leftarrow \tilde{A}$
L		-500 ± 40	$^3\Pi_1 \leftarrow \tilde{A}'$
M		-230 ± 30	$^3\Pi_1 \leftarrow \tilde{A}$ and $^3\Pi_2 \leftarrow \tilde{X}'\,^2\Pi_{1/2}$[a]
N	1.940 ± 0.005	0	$^3\Pi_2 \leftarrow \tilde{X}\,^2\Pi_{3/2}$
O		125 ± 40	$^3\Pi_1 \leftarrow \tilde{X}'\,^2\Pi_{1/2}$
P		405 ± 30	$^3\Pi_1 \leftarrow \tilde{X}\,^2\Pi_{3/2}$
Q	2.103 ± 0.005	0	—
R	2.404 ± 0.005	0	$^3\Phi_4, ^3\Delta_3$, or $^3\Pi_2 \leftarrow \tilde{X}\,^2\Pi_{3/2}$[a]
S		575 ± 30	$^3\Phi_3, ^3\Delta_2$, or $^3\Pi_1 \leftarrow \tilde{X}\,^2\Pi_{3/2}$[a]
T		1130 ± 30	$^3\Phi_2, ^3\Delta_1$, or $^3\Pi_0 \leftarrow \tilde{X}\,^2\Pi_{3/2}$[a]
U		-640 ± 30	$^1\Pi_1 \leftarrow \tilde{A}$
V		-265 ± 30	$^1\Pi_1 \leftarrow \tilde{X}'\,^2\Pi_{1/2}$
W	2.706 ± 0.005	0	$^1\Pi_1 \leftarrow \tilde{X}\,^2\Pi_{3/2}$

[a] See text for details.

Peak N is the most intense peak in the spectrum and is located 0.485 eV above peak D (Table 1). Peak P falls nearby at 0.536 eV above peak D. As was stated above, σ electron detachment is expected to yield the highest intensity peaks. In this case, σ electron detachment from $1\delta^4 2\pi^3 2\sigma^2$ NiO^- gives a $^3\Pi$ state. In a fluorescence detection experiment, Friedman-Hill and Field (*11*) show the $^3\Pi_2$ state to be 0.484 eV above the ground state and the $^3\Pi_1$ state at 0.533 eV. These measurements coincide with the observed spacing between peaks N and D and P and D, securely fixing the assignment of the $^3\Pi_2$ and $^3\Pi_1$ and $^3\Sigma^-$ states (Tables 1 and 2). Therefore, peak D corresponds to the electron affinity transition, with $EA(NiO) = 1.455 \pm 0.005$ eV. This value is reasonably consistent with those determined by Wu and Wang (*15*) at 1.46(2) eV and Moravec and Jarrold (*16*) at 1.470(3) eV. Moravec and Jarrold also find the $^3\Pi_1$ electronic state at 0.532 eV excitation energy, in agreement with our assignment. Wu and Wang observe this transition, but discount the Friedman-Hill and Field (*11*) measurement, as they assign the 0.49-eV peak to the NiO $^3\Pi_1$ state and a 0.55-eV peak to the $^3\Pi_0$ state. This assignment results in assigning their 0.43-eV peak as the $^3\Pi_2$ state, as opposed to the anion excited

TABLE 2
Summary of Assignments for NiO and NiO^-

		Relative Energy (eV)	T_e (eV)	r_e (Å)
NiO^-	$\tilde{X}\,^2\Pi_{3/2}$	−1.455(5)	0	1.66(1)
	$\tilde{X}'\,^2\Pi_{1/2}$		0.034(5)	
	$\tilde{A}$		0.081(4)	
	$\tilde{A}'$		0.113(4)	
NiO	$^3\Sigma^{-c}$	0	0	1.627[a]
	?		0.313(5)	1.66(1)
	$^3\Pi_2$		0.485(5)	1.645[a]
	$^3\Pi_1$		0.536(5)	1.645[a]
	?		0.648(5)	1.66(2)
	$^3\Phi_4$, $^3\Delta_3$, or $^3\Pi_2$[b]		0.949(6)	1.66(2)
	$^3\Phi_3$, $^3\Delta_2$, or $^3\Pi_1$[b]		1.020(7)	1.66(2)
	$^3\Phi_2$, $^3\Delta_1$, or $^3\Pi_0$[b]		1.089(6)	1.66(2)
	$^1\Pi_1$		1.251(6)	1.66(2)

[a] Refs. (*10, 12, 13*).
[b] See text for details.
[c] $\nu = 825\ cm^{-1}$.

state assignment offered below. The $405 \pm 30\ cm^{-1}$ spacing between the $^3\Pi_2$ and $^3\Pi_1$ peaks gives the neutral NiO spin–orbit splitting (see Table 7). There is a very weak unlabeled peak at 2.038 eV binding energy, between peaks P and Q. While the location of this peak is appropriate for the $^3\Pi_0 \leftarrow {}^2\Pi_{3/2}$ transition, the fact that other peaks in the spectrum with comparable intensity are unassigned leads us not to claim its assignment. This $^3\Pi_0 \leftarrow {}^2\Pi_{3/2}$ transition involves a change in Ω of 3/2, which will make the transition weaker, but it is still allowed, as elaborated in the following discussion.

Many of the intense transitions identified in all of these spectra involve photodetachment of a σ electron from a $2\pi^3 2\sigma^2\,{}^2\Pi_{3/2,1/2}$ anion, resulting in neutral $^3\Pi_{2,1,0}$ states. The transitions identified include both $^3\Pi_0 \leftarrow {}^2\Pi_{3/2}$ and $^3\Pi_2 \leftarrow {}^2\Pi_{1/2}$ transitions, where there is a change of $\frac{3}{2}\hbar$ in the component of angular momentum along the internuclear axis, Ω. In earlier studies, Ho *et al.* (*57*), Neumark and co-workers (*58, 59*), and Moravec *et al.* (*60*) have pointed out a $\Delta\Omega = \pm\frac{1}{2}$ selection rule for σ electron detachment from a $\pi^3 2\sigma^2$ configuration. This selection rule effectively comes from the observation that only p-wave electron detachment is possible for a one-electron process involving an electron in a σ_g orbital. The molecular symmetry basis for this restriction is cogently described by Moravec *et al.* (*60*). All of the examples of this selection rule involve homonuclear diatomic molecules, where inversion symmetry provides a good quantum number. For these metal oxides, the σ orbitals arise from mixing an O2p_z orbital with metal s or d orbitals, resulting in σ orbitals with substantial gerade *and* ungerade character. Detachment of an electron from a σ_u orbital gives s and d wave contributions, and the selection rule above is not applicable in this case. The experimental observation that the photoelectron angular distributions for the Π states of the metal oxides are much less strongly peaked along the laser electric vector than for Pb_2 or Sn_2 (*61*) provides confirmation of this analysis.

Peak G lies 825 cm^{-1} above peak D (Table 1), an interval that is the same as the vibrational frequency values measured by several others: argon-matrix-isolated NiO (825.74 cm^{-1} (*9*) and 825.7 cm^{-1} (*14*)), laser-induced fluorescence (839.69 cm^{-1} (*11*)), and anion photoelectron spectroscopy (840 cm^{-1} (*16*) and 800 cm^{-1} (*15*)). Peak G, therefore, is assigned as the first quantum of the NiO stretch. A 0.03 ± 0.01-Å change in bond length (Δr_e) is obtained from a Franck–Condon fit to the $v = 0$ and $v = 1$ peak intensities. As the detached electron arises from an antibonding orbital, the known NiO ground state bond length (1.627 Å (*10, 12, 13*)) gives an anion bond length of 1.66 ± 0.01 Å. As discussed below, peak G is the only manifestation of vibrational activity in the NiO^- photoelectron spectrum. This 1.66-Å anion bond length is consistent with the absence of a detectable vibrational progression for the $^3\Pi_{2,1}$ states, with a bond length of 1.627 Å (*11*). The remaining peaks are all $\Delta v = 0$ transitions with $\Delta r_e < 0.02$ Å (see Table 2).

Peaks C, B, and A are spaced 275, 650, and 910 cm^{-1}, respectively, above the origin, peak D. They appear to be anion hot bands, but none of the frequencies are close to that expected for the anion vibration ($\sim$800 cm^{-1}) and their intensity relative to that of peak G precludes the assignment of any of them to anion vibrations. Elaborating, the intensity of the $(v = 1)\,{}^3\Sigma^- \leftarrow (v' = 0)\,{}^2\Pi_{3/2}$ peak G, $I(1, 0)$, relative to that of the origin peak, $I(0, 0)$, is determined by the magnitude of the $\langle 1|0\rangle^2$ Franck–Condon factor:

$$\frac{I(1,0)}{I(0,0)} = \langle 1|0\rangle^2. \qquad [1]$$

In the harmonic oscillator approximation, $\langle 1|0\rangle^2 = \langle 0|1\rangle^2$ if the anion and neutral vibrational frequencies are essentially the same, as is the case for a nonbonding electron. The intensity of the $(v = 0)\,{}^3\Sigma^- \leftarrow (v' = 1)\,{}^2\Pi_{3/2}$ peak relative to the origin peak depends on both the $\langle 0|1\rangle^2$ factor and the relative populations of the anion $v = 0$ and $v = 1$ states

$$\frac{I(0,1)}{I(0,0)} = \frac{N(v=1)}{N(v=0)}\langle 1|0\rangle^2. \qquad [2]$$

Given the fact that the intensity of peaks A–C is comparable to that of peak G, this means that if any of peaks A–C arise from vibrational hot bands, then

$$\frac{I(1,0)}{I(0,0)} \cong \frac{I(0,1)}{I(0,0)}. \qquad [3]$$

Equations [2] and [3] imply that the population needed in the anion $v' = 1$ state would have to be comparable to that in $v' = 0$, which is not likely, given the high pressure and cooling available in our ion source. Thus the intensity of peaks A–C is too great to ascribe them to vibrational hot bands, as they were assigned by Wu and Wang (*15*). Rather, we believe that they arise from

transitions from electronically excited NiO^- states. NiO has considerable ionic character and the $^2\Pi$ anion may be considered Ni–O^- (*11*). Therefore the spin–orbit splitting would be expected to be on the order of the O^- spin–orbit splitting, 180 cm^{-1} (*52*), as opposed to the Ni^- spin–orbit splitting, 1500 cm^{-1}. The 275 cm^{-1} splitting observed here (Table 7) is in the range to be expected for the $^2\Pi_{3/2}$–$^2\Pi_{1/2}$ spacing of NiO^-. Thus peak C is assigned as the $^3\Sigma^- \leftarrow \tilde{X}'\,^2\Pi_{1/2}$ transition, in agreement with Moravec and Jarrold (*16*).

Peaks A and B, therefore, must result from transitions originating in another anion-excited electronic state. Peak B is located 650 cm^{-1} from the electron affinity peak (Table 1) and is assigned as an unspecified $\tilde{A}$ state in the anion. Peak A is 260 cm^{-1} to the lower binding energy side of the $^3\Sigma^- \leftarrow \tilde{A}$ transition, which is similar to the anion $^2\Pi_{3/2}$–$^2\Pi_{1/2}$ spacing. Thus it is possible that peak A is the spin–orbit excited counterpart of this $^3\Sigma^- \leftarrow \tilde{A}$ peak. One possible orbital configuration of this anion-excited electronic state $\tilde{A}$ arises from the promotion of both 2σ electrons to the 3σ orbital (Fig. 1), which would produce a $^2\Pi_{3/2}$ state with a $1\delta^4 2\pi^3 3\sigma^2$ configuration. This excited electronic state should have a $^2\Pi_{3/2}$–$^2\Pi_{1/2}$ splitting on the same order as that of the anion ground state splitting, as we observe here. Other possibilities include a $2\pi^3 2\sigma^2\ 3\sigma\ 4\Sigma$ metastable state and the spin–orbit components of $2\sigma^1 3\sigma^{1,2,4}\Pi$ states. The significant configuration mixing likely between the 2σ and 3σ orbitals means that none of these possibilities can be excluded based solely upon our data. With the information available to us, a definite assignment is not possible. Our assignment of the spin–orbit excited state (peak C) is in agreement with that of Jarrold (*16*), as is the indication of another electronically excited state (peak A).

Peak E, 190 cm^{-1} from the *EA* peak, arises from the $^3\Sigma^-(v=1) \leftarrow \tilde{A}$ transition. Peak F is 825 cm^{-1} from peak C and is assigned as $\tilde{X}\,^3\Sigma^-(v=1) \leftarrow \tilde{X}'\,^2\Pi_{1/2}$. Peak H is 1055 cm^{-1} from peak D and is most likely the $\tilde{X}\,^3\Sigma^-(v=2) \leftarrow \tilde{A}$ transition. Peak I, at a 0.313-eV term energy (Table 1), has an isotropic angular distribution, and its relatively low intensity suggests detachment from a δ orbital. Walch and Goddard (*19*) calculate a $^1\Delta$ as the first excited state, although later calculations by Bauschlicher *et al.* (*62*) place this state at much higher energies. Our data do not permit assignment of this state beyond noting that the unique angular distribution is indicative of detachment from an orbital different from all of the others except peak Q.

As stated above, peaks N and P correspond to transitions from $\tilde{X}$ NiO^- into $^3\Pi_2$ and $^3\Pi_1$ NiO, respectively. As shown in Table 1, peaks J–M and O are analogous to peaks A–C, discussed above. For further discussion, see Ref. (*49*).

Peak Q, 0.648 eV above the *EA* transition, has the other isotropic ($\beta = 0$) angular distribution observed in the spectrum. A possible δ-electron detachment assignment is the $^3\Phi$ state that Bauschlicher *et al.* (*17*) calculate at 0.720 eV. Moravec and Jarrold (*16*) assign this peak as the $^3\Phi_3$ state, and they find a second peak at 0.77 eV excitation energy that they ascribe to the $^3\Phi_2$ state. This latter peak is absent in our spectrum, and, without further theoretical guidance, we have no assignment for peak Q.

Peaks R, S, and T form a uniformly spaced set of peaks at 0.949, 1.020, and 1.089 eV excitation energy. Both Moravec and Jarrold (*16*) and Wu and Wang (*15*) observe this group of peaks and ascribe them to a vibrational progression in a $^1\Delta$ NiO state. This assignment is not consistent with a Franck–Condon analysis, however. If peaks R, S, and T composed a $v = 0$, 1, 2 vibrational progression, these intensities would imply a large change in bond length (>0.1 Å), which would in turn predict a substantial $v = 3$ peak, located between peaks T and U, at 1.17 eV excitation energy. Because such a peak is not observed, peaks R–T are instead assigned as transitions into a triplet NiO state. The intensity of peaks R–T is smaller than that of most of the other peaks in the spectrum, making σ electron detachment unlikely. Possible candidates for the assignment of this triplet include a $^3\Delta$ state that would arise from π electron detachment (*17*) or the $^3\Phi$ (*17, 23*) or $^3\Pi$ states (*19*) created by detaching a δ electron. Because more data are needed to choose between these potential assignments, peaks R, S, and T may be assigned to any of these three triplet states (Tables 1 and 2).

Peaks U, V, and W are a fairly intense ensemble of peaks with peak W 1.251 eV above the electron affinity peak (Table 1). The observed spacing between peaks W and V (265 cm^{-1}) and W and U (640 cm^{-1}) indicates that the assignment of these peaks should be analogous to that of peaks D, C, and B (see Table 1), rather than the $^3\Pi \leftarrow {}^2\Pi_{3/2}$ assignment in Moravec and Jarrold (*16*) or the $^3\Phi$ assignment by Wu and Wang (*15*). The appearance of these 265 and 640 cm^{-1} spacings throughout the spectrum has been discussed, but their assignment to anion electronic state excitation is truly anchored in peaks U and V, where only simple inspection of their intensities with respect to peak W rules out anion vibrational excitation. The intensity of peak W with respect to others in this spectrum suggests that it arises from detachment of a σ electron, and it is assigned as a $^1\Pi \leftarrow {}^2\Pi_{3/2}$ transition.

A summary of results for the photoelectron spectrum of NiO^- is given in Table 2. In this spectrum we have identified transitions from four electronic states of the anion, the ground $\tilde{X}\,^2\Pi_{3/2}$ state and its spin–orbit excited $\tilde{X}'\,^2\Pi_{1/2}$ state at 275 cm^{-1} (Table 7), plus two additional unidentified ($\tilde{A}$ and $\tilde{A}'$) electronic states at higher excitation energies. In neutral NiO, the ground $^3\Sigma^-$ state is observed and the electron affinity is 1.455 eV. The $^3\Pi$ and $^1\Pi$ states are assigned as well as another triplet state, either a $^3\Phi_{4,3,2}$, a $^3\Delta_{3,2,1}$, or a $^3\Pi_{2,1,0}$ state. The $^3\Pi_2$ and $^3\Pi_1$ spin–orbit spacing is 405 cm^{-1} (Table 7). A 825 cm^{-1} vibrational frequency was found for the NiO ground state, as well as a bond length change of 0.03 Å, yielding an anion bond length of 1.66 Å.

PdO

The 364-nm cold photoelectron spectrum of PdO^- recorded at magic angle polarization is shown in Fig. 3. This is an

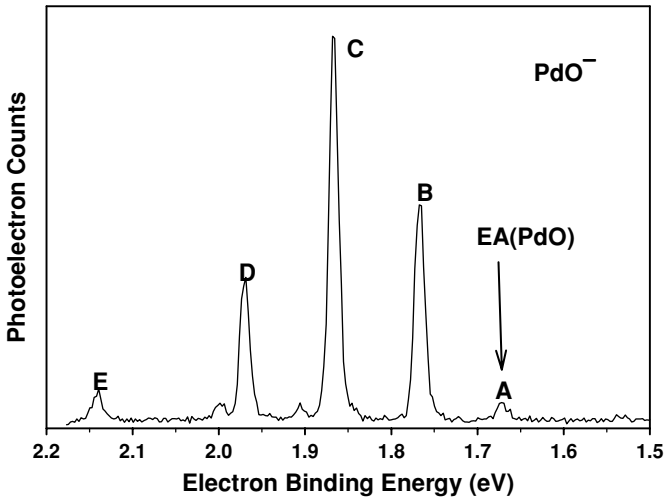

FIG. 3. 364-nm photoelectron spectrum of the onset region of PdO^- taken at magic angle polarization and flow tube temperature 200 K.

TABLE 3
Absolute and Relative Positions, Anisotropy Parameters (β), and Assignments for Peaks in the Photoelectron Spectrum of PdO^-

Peak	Binding Energy (eV)	Relative Position (cm^{-1})	β	Assignment
A′		-335 ± 30		$\tilde{X}\,^3\Sigma^- \leftarrow \tilde{X}'\,^2\Pi_{1/2}$
A	1.672 ± 0.005	0	0.4 (2)	$\tilde{X}\,^3\Sigma^- \leftarrow \tilde{X}\,^2\Pi_{3/2}$
B′		-340 ± 40		$^3\Pi_2 \leftarrow \tilde{X}'\,^2\Pi_{1/2}$
B	1.767 ± 0.005	0	0.8 (1)	$^3\Pi_2 \leftarrow \tilde{X}\,^2\Pi_{3/2}$
C′		-330 ± 30		$^3\Pi_1 \leftarrow \tilde{X}'\,^2\Pi_{1/2}$
C	1.867 ± 0.005	0	1.5 (1)	$^3\Pi_1 \leftarrow \tilde{X}\,^2\Pi_{3/2}$
D′		-345 ± 40		$^3\Pi_0 \leftarrow \tilde{X}'\,^2\Pi_{1/2}$
D	1.970 ± 0.005	0	1.1 (1)	$^3\Pi_0 \leftarrow \tilde{X}\,^2\Pi_{3/2}$
E′		-390 ± 40		$^1\Delta$, $^1\Sigma$, or $^3\Phi \leftarrow \tilde{X}\,^2\Pi_{1/2}$[a]
E	2.141 ± 0.005	0	1.1 (1)	$^1\Delta$, $^1\Sigma$, or $^3\Phi \leftarrow \tilde{X}\,^2\Pi_{3/2}$[a]
F′		-350 ± 30		$^1\Pi_1 \leftarrow \tilde{X}'\,^2\Pi_{1/2}$
F	2.236 ± 0.005	0	1.2 (1)	$^1\Pi_1 \leftarrow \tilde{X}\,^2\Pi_{3/2}$
G′		-350 ± 30		$^3\Phi$ or $^3\Pi \leftarrow \tilde{X}\,^2\Pi_{1/2}$[a]
G	2.454 ± 0.005	0	-0.2 (2)	$^3\Phi$ or $^3\Pi \leftarrow \tilde{X}\,^2\Pi_{3/2}$[a]

[a] See text for details.

expanded spectrum focusing on the lower binding energy range, although a full cold scan was also taken (not shown). There are several peaks of various intensities within a relatively small energy range, as was the case for NiO^-, although the density of peaks is considerably less than for NiO^-.

The orbital configuration for PdO^- may be treated as similar to that of NiO^- (see Fig. 1), with a $1\sigma^2 1\pi^4 1\delta^4 2\pi^3 2\sigma^2$ configuration and a $^2\Pi_{3/2}$ ground state. There has not been a clear determination of the PdO ground state. Elaborate calculations of low-lying PdO electronic states show that the $1\delta^4 2\pi^2 2\sigma^2$ configuration $^3\Sigma^-$ and $1\delta^4 2\pi^3 2\sigma^1$ configuration $^3\Pi$ states lie very close in energy (*18, 24–29*), but cannot conclude which is the ground state. Peak A is weak, so it does not originate from the σ-electron detachment that would produce the $^3\Pi$ state. Rather, the peak is produced from π-electron detachment, resulting in the $^3\Sigma^-$ state. Thus the $^3\Sigma^- \leftarrow {}^2\Pi_{3/2}$ transition is assigned to peak A (see Tables 3 and 4) and corresponds to the electron affinity $EA(\mathrm{PdO}) = 1.672 \pm 0.005$ eV.

Klopcic *et al.* (*31*) have recently reported the photoelectron spectrum of PdO^- using a laser ablation ion source and a time-of-flight electron energy analyzer with energy resolution roughly 5–50 meV. The peaks in their photoelectron spectrum qualitatively match ours with one exception. Klopcic *et al.* observe a peak at binding energy 1.570 eV that they take to be the electron affinity. This peak is absent in our spectrum (see Fig. 3) and as outlined below, we differ in our assignment of the *EA*.

Peak B is located 0.095 eV above the *EA* transition (Table 3). It has a β of 0.8, which contrasts with that of peak A (0.4), and confirms that peaks A and B represent two different PdO electronic states. Peak B, therefore, is assigned as $^3\Pi \leftarrow {}^2\Pi_{3/2}$. The approximately 100-meV energy difference between the $^3\Pi$ and $^3\Sigma^-$ states in neutral PdO is consistent with calculations (*18, 24–29*) that predict the two states to be close in energy. Furthermore, peak B is the second most intense peak in the spectrum, so it is expected to result from the σ-electron detachment necessary to produce a $^3\Pi$ state in PdO.

Peaks B, C, and D form a trio of intense peaks. They all have similar angular distributions ($\beta \approx 1$) and are evenly spaced, but do not constitute a vibrational progression. Such a progression would arise from a relatively large change in bond length that would also produce vibrational hot bands, which we do not observe. Second, and more importantly, efforts to simulate these peaks as a vibrational progression using a Franck–Condon fitting routine (*55*) failed. The bond length change necessary results in a large $v = 3$ peak between peaks D and E; no such peak appears in our spectrum (see Fig. 3). So, while the approximately 100-meV separation between peaks B, C, and D could equally well have represented either the PdO vibrational frequency or the spin–orbit splitting, the modeling rules out the former. Thus B, C, and D are ascribed to $^3\Pi_{2,1,0} \leftarrow {}^2\Pi_{3/2}$ transitions,

TABLE 4
Summary of Assignments for PdO and PdO^-

		Relative Energy (eV)	T_e (eV)
PdO^-	$^2\Pi_{3/2}$	$-1.672(5)$	0
	$^2\Pi_{1/2}$		0.041
PdO	$^3\Sigma^-$	0	0
	$^3\Pi_2$		0.095
	$^3\Pi_1$		0.195
	$^3\Pi_0$		0.298
	$^1\Delta$, $^1\Sigma$, or $^3\Phi$		0.469
	$^1\Pi_1$		0.564
	$^3\Phi$ or $^3\Pi$		0.782

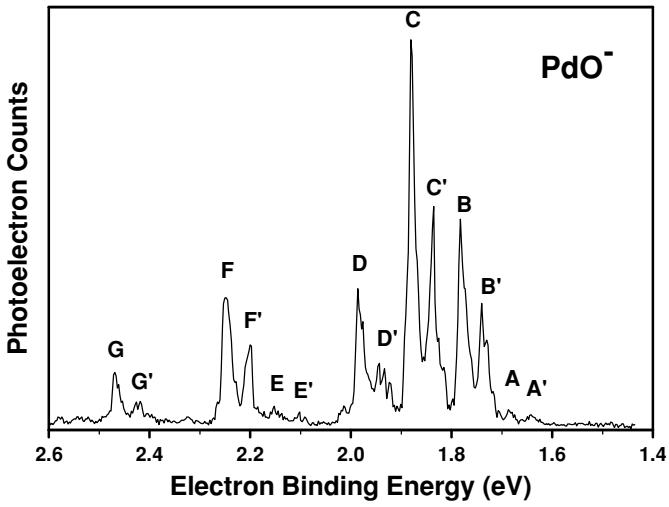

FIG. 4. 364-nm magic angle photoelectron spectrum of PdO^- taken at flow tube temperature 300 K.

respectively (Table 3). The neutral PdO $^3\Pi_2$–$^3\Pi_1$ spin–orbit splitting is 805 ± 20 cm^{-1} (Table 7).

Peak E is a rather weak transition located at excitation energy 0.469 eV (Table 3). Its intensity eliminates a $^1\Pi$ state assignment, which would result from detaching a σ electron and would have a relatively large cross-section for detachment. Possible assignments include the $^3\Phi$ or $^1\Delta$ states formed by detaching a δ electron or a $^1\Sigma^+$ state (*24*). The small peaks to the higher binding energy side of peaks C and D are left unassigned.

Peaks F and G, which are observed in the cold full scan (not shown), are visible in the warm spectrum shown in Fig. 4, discussed below. Peak F, at 0.564 eV above the $^3\Sigma^- \leftarrow {}^2\Pi_{3/2}$ (Table 3), has intensity comparable to that of the $^3\Pi_{2,1,0} \leftarrow {}^2\Pi_{3/2}$ peaks and a similar β ($\approx$1). The height of the peak, as well as its angular distribution, points to σ-electron detachment in its formation. Therefore peak F is assigned to the $^1\Pi_1 \leftarrow {}^2\Pi_{3/2}$ transition.

Peak G, with excitation energy 0.782 eV, has an isotropic angular distribution and is relatively weak. This suggests δ-electron detachment and possible final states include $^3\Phi$ and $^1\Phi$ or $^3\Pi$ or $^1\Pi$. Hund's rules would predict the triplet states to lie at lower energy, favoring a $^3\Phi$ or $^3\Pi$ state (Tables 3 and 4).

The 364-nm magic angle photoelectron spectrum of warm PdO^- is displayed in Fig. 4. Comparing Figs. 3 and 4 shows that every feature A–E in the cold spectrum is now a doublet, with a second weaker feature appearing about 330 cm^{-1} to lower binding energy. The same is true for F and G, although the data are not shown here. These "new" peaks, which are obviously temperature dependent, are labeled A′–G′ in Fig. 4. The intensities of peaks A′–G′ are too great with respect to those of their unprimed counterparts to result from a vibrationally excited anion state, especially with the complete lack of transitions into vibrationally excited neutral PdO. Furthermore, the spacing between primed and unprimed peaks is 330 ± 30 cm^{-1}, which is too small for the stretching vibration. Thus the primed peaks originate from an electronically excited anion state, either the $^2\Pi_{1/2}$ spin–orbit excited state or another low-lying excited electronic state.

The spin–orbit excited state is the most likely explanation. The ionic nature of the Ni–O bond allowed a first-order estimate for the anion spin–orbit splitting (close to the splitting of O^-). That line of reasoning is not guaranteed to be applicable to PdO. However, a different argument is proposed as to why the 330 cm^{-1} spacing between primed and unprimed peaks is expected as a spin–orbit splitting in PdO^-. The electron affinity of Pd^- is around 0.5 eV. This is relatively low, testifying to the low electronegativity of Pd. Thus in the PdO^- molecule, the extra electron would be expected to be more localized on the oxygen atom and so the spin–orbit splitting of PdO^- would be closer to the value of atomic O^- ($\approx$200 cm^{-1}) than the Pd^- value ($\approx$3000 cm^{-1} (*63*)). The primed peaks are therefore ascribed to transitions from the anion spin–orbit excited $^2\Pi_{1/2}$ state.

In the photoelectron spectra of both NiO^- and PdO^- we identify anion $^2\Pi_{3/2}$ and $^2\Pi_{1/2}$ transitions into both $^3\Pi$ and $^1\Pi$ neutral states. The neutral spin–orbit splittings, about 400 cm^{-1} for NiO and 800 cm^{-1} for PdO (Table 7), correlate well with the trends found for CuO (279 cm^{-1}) (*41*) and AgO (269 cm^{-1}) (*64, 65*) for two reasons. First, the CuO and AgO splittings resemble more the atomic oxygen spin–orbit splitting (hundreds of cm^{-1}) rather than that of the metal atom (thousands of cm^{-1}), as is the case for NiO and PdO. Second, there is not a significant difference in the magnitude of the splitting going from CuO to AgO; in NiO and PdO, although the neutral spin–orbit splitting does double, the values still are closer to the O^- splitting than those of the metal anion.

As noted in the NiO discussion, one might expect the $^3\Pi_0 \leftarrow {}^2\Pi_{3/2}$ transition to be weaker than the corresponding transitions to $^3\Pi_2$ or $^3\Pi_1$. The peak that we ascribe to the $^3\Pi_0 \leftarrow {}^2\Pi_{3/2}$ transition (D) is more intense relative to the other spin–orbit components than in the NiO spectrum, but not enough to cast doubt on the assignment. Simple arguments based upon the greater admixture of ungerade character for the detached σ electron in PdO relative to NiO account for the increased intensity. What may be more problematic is the observation made by the referee that the assignment of peak D to $^3\Pi_0 \leftarrow {}^2\Pi_{3/2}$ makes the PdO spin–orbit levels uniformly spaced, implying that the position of the $^3\Pi_1$ level is relatively unperturbed. A simple argument suggests that the nearby $^1\Pi_1$ state (peak F, 0.37 eV higher in energy) should perturb the $^3\Pi_1$ level significantly, rendering the multiplet splitting nonuniform. The shift observed for NiO (*11*) is about 3 cm^{-1}, but for NiO the corresponding perturbing level is about 1.5 eV higher in energy. While it is clearly conceivable that peak F corresponds to another NiO electronic state, such an assignment leaves a missing transition to $^3\Pi_0$. The assignment reported here appears to be the most plausible alternative.

The assignments extracted from the photoelectron spectrum of PdO are summarized in Table 4. Both the $^2\Pi_{3/2}$ and $^2\Pi_{1/2}$ PdO^- states, as well as PdO $^3\Pi$ and $^1\Pi$ states, are identified.

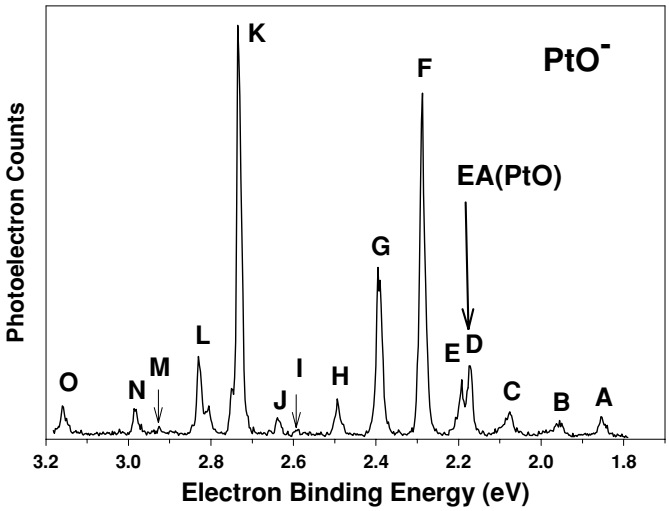

FIG. 5. 364-nm magic angle photoelectron spectrum of PtO^- taken at flow tube temperature 200 K.

The ground state of PdO was found to be $^3\Sigma^-$, as in NiO, and $EA(PdO) = 1.672 \pm 0.005$ eV. Two other excited PdO states were observed, one being either a $^1\Delta$, $^1\Sigma$, or $^3\Phi$ state and the other either a $^3\Pi$ or $^3\Phi$ state. No vibrational progressions were observed for any transitions. The anion $^2\Pi_{3/2}$–$^2\Pi_{1/2}$ splitting is 330 cm^{-1} while the neutral $^3\Pi_2$–$^3\Pi_1$ splitting is 805 cm^{-1} (see Table 7).

PtO

Very little is known about the low-lying states of PtO to assist in assignment of the photoelectron spectrum. The ground state is a $^3\Sigma^-_{0^+}$ state with the related $^3\Sigma^-_1$ state lying 936 cm^{-1} higher (*35*). Frum and co-workers (*37*) observed an $A'\,^3\Pi_{0,1,2}$ state with a $\delta^3\pi^3\sigma^2$ configuration with a measured $^3\Pi_2$–$^3\Sigma^-_{0^+}$ splitting of 8935 cm^{-1} (1.108 eV). These are the only known states that might be accessible with 364-nm excitation of the PtO-anion, and the transition producing the Π state should be quite weak, as it involves detachment of a δ electron. The cold photoelectron spectrum PtO^- recorded at magic angle laser polarization is displayed in Fig. 5. As was the reasoning for the photoelectron spectra of NiO^- and PdO^-, detaching a σ electron is expected to have a large cross section and therefore yield an intense photoelectron peak. If the $1\delta^4 2\pi^3 2\sigma 2$ orbital configuration for PtO^- is valid (as for NiO and PdO in Fig. 1), this corresponds to production of PtO $^{1,3}\Pi$ states. Thus peaks F and K arise from transitions producing Π electronic state(s). In analogy to the assignment in NiO^- and PdO^-, peak F is assigned as the transition into the $1\delta^4 2\pi^3 2\sigma^1$ configuration $^3\Pi_2$ state.

It is natural to suppose that peaks G and H are transitions into the $^3\Pi_1$ and $^3\Pi_0$ neutral states; however, this is not the case. Instead, peaks E, F, G, H, and I correspond to vibrational levels of the $^3\Pi_2 \leftarrow {}^2\Pi_{3/2}$ transition. Because peak E, which is 770 cm^{-1} from peak F, has an intensity that varies with the anion temperature, it is assigned to the $v' = 1$ transition from the anion (see Tables 5 and 6). Peaks G, H, and I are transitions into the $v = 1, 2$, and 3 levels in $^3\Pi_2$ PtO, respectively. This conclusion is verified in several ways. First, the angular distributions for peaks E–H are equal ($\beta \approx 1.0$), indicating they all arise from detachment out of the same orbital. Second, the angular distributions of peaks A through D have contrasting values ($\beta < 1$) and thus are not associated with peaks E–I. In addition, if peaks G and H were actually $^3\Pi_1$ and $^3\Pi_0$ states rather than the $v = 1$ and $v = 2$

TABLE 5
Absolute and Relative Positions, Anisotropy Parameters (β), and Assignments for the Photoelectron Spectrum of PtO^-

Peak	Binding Energy (eV)	Relative Position (cm^{-1})	Energy Difference from Peak F (cm^{-1})	β	Assignment[a]
A	1.851 (5)	0	−3510 (40)	0.4 (2)	$^3\Pi_2 \leftarrow {}^2\Pi_{1/2}$
B		855 (40)	−2655 (40)	0.3 (2)	$(v=1)\,^3\Pi_2 \leftarrow {}^2\Pi_{1/2}$
C		−770 (40)	−1695 (40)	0.0 (2)	$^3\Sigma^-_{0^+} \leftarrow (v=1)\,\tilde{X}\,^2\Pi_{3/2}$
D	2.172 (5)	0	−930 (0)	0.0 (1)	$^3\Sigma^-_{0^+} \leftarrow \tilde{X}\,^2\Pi_{3/2}$
E		−770 (30)	−770 (30)	0.9 (1)	$^3\Pi_2 \leftarrow (v=1)\tilde{X}\,^2\Pi_{3/2}$
F	2.287 (5)	0	0	0.9 (1)	$^3\Pi_2$ and $^3\Sigma^-_1 \leftarrow \tilde{X}^2\Pi_{3/2}$
G		845 (30)	845 (30)	1.1 (1)	$(v=1)\,^3\Pi_2 \leftarrow \tilde{X}\,^2\Pi_{3/2}$
H		1655 (30)	1655 (30)	1.1 (1)	$(v=2)\,^3\Pi_2 \leftarrow \tilde{X}\,^2\Pi_{3/2}$
I		2450 (30)	2450 (30)	—	$(v=3)\,^3\Pi_2 \leftarrow \tilde{X}\,^2\Pi_{3/2}$
J		−765 (40)	2815 (40)	0.4 (2)	$(v=0)\,^3\Pi_1 \leftarrow (v=1)\tilde{X}\,^2\Pi_{3/2}$
K	2.731 (5)	0	3580 (30)	1.1 (1)	$(v=0)\,^3\Pi_1 \leftarrow \tilde{X}\,^2\Pi_{3/2}$
L		780 (30)	4360 (30)	1.2 (1)	$(v=1)\,^3\Pi_1 \leftarrow \tilde{X}\,^2\Pi_{3/2}$
M		1565 (40)	5145 (40)	—	$(v=2)\,^3\Pi_1 \leftarrow \tilde{X}\,^2\Pi_{3/2}$
N	2.982 (5)	0	0	1.0 (2)	—
O	3.157 (5)	0	0	0.2 (2)	—

[a] All states are $v = 0$ unless otherwise specified.

TABLE 6
Summary of Assignments for PtO and PtO^-

		Relative Energy (eV)	T_e (eV)	ν (cm^{-1})	r_e (Å)
PtO^-	$^2\Pi_{3/2}$	−2.172(5)	0	770	r_{PtO-}
	$^2\Pi_{1/2}$		0.321(5)		
PtO	$^3\Sigma^-_{0^+}$	0	0		1.736[a]
	$^3\Sigma^-_1$		0.116[a]		1.736[a]
	$^3\Pi_2$		0.115(5)	845	$r_{PtO-} - 0.05(1)$[b]
	$^3\Pi_1$		0.559(5)	780	$r_{PtO-} - 0.035(10)$[b]
	?		0.810		
	?		0.985		

[a] Measurement of $^3\Sigma^-_{0^+}$–$^3\Sigma^-_1$ splitting and bond length from Refs. (*35*), (*36*) and (*37*).
[b] See text for details.

of the $^3\Pi_2$ state, then there would be no observed vibrational excitation of PtO. Given the intensity of the anion vibrational hot band peak E, using a Franck–Condon argument similar to that outlined in Eqs. [1]–[3] would estimate an anion population in the $v = 1$ state 10 times greater than that in the $v = 0$ state (*49*), which is unreasonable. Thus we are forced to conclude that peaks F–I form a vibrational progression in $^3\Pi_2$ PtO.

To further support this conclusion, the intensities and positions of peaks E–I are well reproduced using a harmonic-oscillator-approximation Franck–Condon fitting routine (*55*). The anion has a 770 cm^{-1} fundamental frequency, and the neutral fundamental frequency is 845 cm^{-1} (Table 5). These values are used in the simulation to determine a Pt–O bond length shortening of 0.05 ± 0.01 Å upon electron detachment from PtO^-, which is larger than the Δr_e measured in NiO. The detached electron is expected to be in an antibonding orbital (see Fig. 1), as is supported by the fact that the anion frequency is smaller than the neutral frequency. Therefore the removal of the electron shortens the PtO bond length.

Because in the photoelectron spectra of NiO^- and PdO^- we observe transitions into both the neutral $^3\Pi_2$ and $^3\Pi_1$ electronic states, we expect the same for PtO^-. Peaks J, K, L, and M are therefore attributed to $^3\Pi_1 \leftarrow {}^2\Pi_{3/2}$ transitions. Like the $^3\Pi_2 \leftarrow (v' = 1)\ ^2\Pi_{3/2}$ peak, peak J has an intensity dependent on the source temperature and is assigned as the $v' = 1$ transition from the anion. Peaks L and M represent transitions into the $v = 1$ and 2 PtO levels, respectively. Peaks K and L both have angular distributions of approximately 1.1. Like peaks E–I, both the intensities and positions of peaks J–M are accurately reproduced using a Franck–Condon fitting routine. The anion fundamental frequency is 765 cm^{-1} (identical to that measured in the $^3\Pi_2 \leftarrow {}^2\Pi_{3/2}$ transition) while the neutral fundamental is 780 cm^{-1} (Table 5). Upon electron detachment the bond length shortens by 0.035 ± 0.010 Å. Again, the anion frequency is smaller than the neutral frequency, although there is a smaller change (15 cm^{-1}) than in the $^3\Pi_2 \leftarrow {}^2\Pi_{3/2}$ case (75 cm^{-1}). This agrees with the smaller bond length change found, and that the observed vibrational progression is less extensive than in the $^3\Pi_2 \leftarrow {}^2\Pi_{3/2}$ case. The PtO $^3\Pi_2$–$^3\Pi_1$ spacing, 3580 ± 20 cm^{-1}, gives the neutral spin–orbit splitting (see Table 7).

This observation of an anion state with excitation energy 3580 cm^{-1} might seem surprising. However, electronic state populations are most definitely not in equilibrium in the flow tube. It has been our repeated experience that, when there is little other than He in the flow tube, metastable electronic states do not reach equilibrium but initially formed metastable electronic states populations do not fully relax in the few ms residence time in the ion source. We of course do not have a definitive identification of the excited state, but it must be metastable, and the $^2\Pi_{1/2}$ PtO^- state represents our most plausible candidate.

As was the case for the PdO^- photoelectron spectrum, there are peaks to the lower binding energy side of the $^3\Pi_2 \leftarrow {}^2\Pi_{3/2}$ peak with smaller intensity and contrasting angular distribution (<1). Peak D is sharp and well defined, while peaks A–C are broad and less intense. The $^3\Sigma^-_{0^+}$ identity of the PtO ground state, which is the same $^3\Sigma^-$ ground state of NiO and PdO, is well established (*27, 34–37*). The first excited state $^3\Sigma^-_1$ of PtO was observed 936 cm^{-1} above the ground state (*35, 36*). The ground state is the 0^+ state while the other is the 1 state in Hund's coupling case c (*66*), both of which correspond to the $^3\Sigma^-_1$ state of PtO (*36, 37*). Peak D is located 930 ± 20 cm^{-1} to the lower binding energy side of the $^3\Pi_2 \leftarrow {}^2\Pi_{3/2}$ peak (Table 5), which matches the observed $^3\Sigma^-_1$–$^3\Sigma^-_{0^+}$ splitting. Peak F therefore is coincident with the $^3\Sigma^-_1$ peak. Peak D is assigned as the electron affinity, $EA(\mathrm{PtO}) = 2.172 \pm 0.005$ eV.

The intensity of peaks A–C relative to the $^3\Pi_2 \leftarrow {}^2\Pi_{3/2}$peak is temperature-dependent, so they originate from anion excited states. Peak C is located 770 cm^{-1} to the lower binding energy side of the $^3\Sigma^-_{0^+} \leftarrow {}^2\Pi_{3/2}$ peak (Table 5), which is the anion $^2\Pi_{3/2}$ fundamental frequency. It also shares the same isotropic angular distribution as the electron affinity peak. Peak C therefore is assigned as the transition from the $v = 1$ anion level to the $^3\Sigma^-_{0^+}$ PtO state. Peak A is located 3510 ± 20 cm^{-1} from the $^3\Pi_2 \leftarrow {}^2\Pi_{3/2}$ peak, and peak B is the same distance from the $(v = 1)\ ^3\Pi_2 \leftarrow {}^2\Pi_{3/2}$ peak. Peaks A and B, therefore, are transitions from the anion spin–orbit excited $^2\Pi_{1/2}$ states into the $v = 0$ and 1 levels of neutral $^3\Pi_2$ PtO, respectively. By analogy, one would expect to see the $(v = 2)\ ^3\Pi_2 \leftarrow {}^2\Pi_{1/2}$ transition, implicating peak C, although this is not completely the case. The

TABLE 7
Anion $^2\Pi_{3/2}$–$^2\Pi_{1/2}$ Spin–Orbit Splittings and Neutral $^3\Pi_2$–$^3\Pi_1$ Spin–Orbit Splittings for the NiO, PdO, and PtO Molecules

	$^2\Pi_{3/2}$–$^2\Pi_{1/2}$	$^3\Pi_2$–$^3\Pi_1$
NiO	275 ± 30 cm^{-1}	405 ± 30 cm^{-1}
PdO	330 ± 30 cm^{-1}	805 ± 30 cm^{-1}
PtO	3510 ± 40 cm^{-1}	3580 ± 40 cm^{-1}

($v = 2$) $^3\Pi_2 \leftarrow {}^2\Pi_{1/2}$ transition would have a smaller intensity than peaks A and B, which is not true for peak C. Also, the spacing between peak C and H is 3350 cm^{-1}, 160 cm^{-1} short of the required spacing. However, there is a small shoulder to the lower binding energy side of peak C that fulfills the required interpeak spacings and is of the expected intensity. Regardless, the ($v = 2$) $^3\Pi_2 \leftarrow {}^2\Pi_{1/2}$ transition should have a small enough intensity (in analogy to the relative intensities of the $v = 0$, 1, and 2 $^3\Pi_2 \leftarrow {}^2\Pi_{3/2}$ peaks) that it blends into the structure of peak C.

Frum and co-workers (*37*) observed a $^3\Pi$ state with a $\delta^3\pi^3\sigma^2$ configuration with a measured $^3\Pi_2$–$^3\Sigma^-_{0^+}$ splitting of 8935 cm^{-1} (1.108 eV). Therefore a peak corresponding to this $^3\Pi_2$ state should be at $1.108 + 2.172 = 3.28$ eV. In addition, a weaker transition to the $^3\Pi_0$ level might appear at 3.19 eV. However, the sensitivity of the electron kinetic energy analyzer drops off for binding energies greater than about 3.2 eV. The fact that we do not see either of these transitions is a consequence of the instrument cutoff and therefore remains consistent with the *EA* $^3\Sigma^-_{0^+}$ assignment of peak D at 2.172 eV.

The electron affinity assignment given here allows the most consistent analysis of the peaks based on literature values. We agree with the 936 cm^{-1} experimental $^3\Sigma^-_1$–$^3\Sigma^-_{0^+}$ splitting of Sassenberg and Scullman (*35, 36*) with the spacing between peaks D and F and observe a repetition of that spacing between peaks E and C. Furthermore, we are consistent with the measurements of Frum *et al.* (*37*) discussed above. If peaks A, B, or C were assigned as the electron affinity, we would disagree with either Frum *et al.* or Sassenberg and Scullman by substantial amounts (>100 cm^{-1}). In addition, with peak A assigned as the $^3\Pi_2 \leftarrow {}^2\Pi_{1/2}$ hot band transition, the anion spin–orbit splitting of 3510 cm^{-1} is similar to the spin–orbit splitting in the neutral PtO (as measured between peaks F and K, 3580 cm^{-1}), as expected. Finally, the 0.115 eV between the $^3\Sigma^-$ and $^3\Pi_2$ states in PtO is nearly equal to that in PdO (0.095 eV). The relative intensities of the $^3\Sigma^- \leftarrow {}^2\Pi_{3/2}$ and $^3\Pi_2 \leftarrow {}^2\Pi_{3/2}$ transitions are also the same between the spectra of PtO^- and PdO^-, as are the relative angular distributions.

Peak N, at excitation energy 0.810 eV (Table 5), remains unassigned. Peak O sits at excitation energy 0.985 eV and has an isotropic angular distribution. This is similar to peak G in the photoelectron spectrum of PdO^- (Fig. 4) because both peaks have similar excitation energy and angular distribution. Consequently, both should receive the same assignment, although it is not clear what that assignment should be.

Like the spectra of NiO^- and PdO^-, the photoelectron spectrum of PtO^- shows transitions from both the anion $^2\Pi_{3/2}$ and $^2\Pi_{1/2}$ states, and a $^3\Sigma^-$ neutral ground state, as summarized in Table 6. PtO $^3\Pi_2$ and $^3\Pi_1$states were also identified, and $EA(\mathrm{PtO}) = 2.172$ eV. An anion vibrational frequency of 770 cm^{-1} was measured, as well as a neutral PtO stretch of 845 cm^{-1} in the $^3\Pi_2$ state and 780 cm^{-1} in the $^3\Pi_1$ state. The bond length is measured to shorten by 0.05 Å for the $^3\Pi_2 \leftarrow {}^2\Pi_{3/2}$ transition while it shortens by 0.035 Å for the $^3\Pi_1 \leftarrow {}^2\Pi_{3/2}$ transition. The anion $^2\Pi_{3/2}$–$^2\Pi_{1/2}$ splitting is 3510 cm^{-1} while the neutral $^3\Pi_2$–$^3\Pi_1$ splitting is 3580 cm^{-1} (Table 7).

Discussion of NiO, PdO, and PtO Data

Spectroscopic studies of NiO by Friedman-Hill and Field (*11*) show that the ground state of NiO is strongly ionic and imply that the anion is formed by adding an essentially nonbonding electron to Ni, giving a zero-order Ni–O^- structure. For both PdO and NiO, the observed spin–orbit splittings in both the $^3\Pi_2$ neutral and the $^2\Pi$ anion are closer to the O^- splitting than the metal spin–orbit splitting (see Table 7). This observation makes a very strong case that both NiO and PdO are strongly ionic, with PdO somewhat less ionic than NiO, based upon its larger spin–orbit splitting. However, the PtO^- spin–orbit splitting of ≈3500 cm^{-1} is more accurately described as roughly halfway between the atomic anion spin–orbit splittings of O^- (180 cm^{-1} (*52*)) and Pt^- (≈9500 cm^{-1} (*67*)). Thus the PtO bond possesses a significantly greater covalent character than either NiO or PdO.

A single peak in the photoelectron spectrum of NiO^- is assigned as vibrational excitation in the neutral ground state. Transitions into the several remaining NiO electronic states display no vibrational excitation and thus originate from detaching essentially nonbonding electrons. For electron detachment from PdO^-, no vibrational excitation is observed, again indicating detachment of only nonbonding electrons. In contrast, in the spectrum of PtO^-, two extended vibrational progressions are observed. These observations are a direct indication of the importance of relativistic effects on the valence orbitals of PtO. The antibonding orbitals from which the anion electrons are detached have become more antibonding than in NiO and PdO. Furthermore, the relativistic contraction of the metal atom *s* orbitals has two important effects. One is that the reduction in size allows better mixing with the oxygen *p* orbitals, rendering the 3σ orbitals no longer primarily nonbonding. Second, the relativistic expansion of the metal *d* orbitals in conjunction with this contraction of the metal *s* orbitals allows better mixing of the characters of the 3σ and the HOMO 2σ orbitals. The shift of the metal 4*s* contribution from nonbonding to antibonding 3σ orbitals and the mixing of the 2σ and 3σ orbitals implies an increased influence of the metal on the HOMO electron properties, testifying to the significant increase in covalent character of the PtO bond with respect to the NiO and PdO bonds.

As explained above, the covalent nature of the PtO bond means that the spin–orbit splitting in both the $2\pi^3 2\sigma^2$anion states and the $2\pi^2 2\sigma^2$ neutral states should approach the mean of the splittings for the individual atoms. For this reason the $^3\Pi_2$–$^3\Pi_1$ splitting increases from 405 cm^{-1} in NiO to 805 cm^{-1} in PdO and to 3580 cm^{-1} in PtO (see Table 7). Thus, peak K must correspond to the transition to the $^3\Pi_2$ state of PtO,

rather than the $^1\Pi$ state. The photoelectron spectra of NiO^- and PdO^- exhibit strong transitions to the $^3\Pi_2$ and $^3\Pi_1$ electronic states. If peak K were assigned as the $^1\Pi$ state, it would leave unanswered the question of where is the $^3\Pi_1$ state, which must be both intense and accessible with 3.408 eV photons. These observations are supported by previous theoretical findings. Chung *et al.* (*27*) performed gradient-corrected density functional calculations incorporating relativistic effects on NiO, PdO, and PtO. They find a change in bonding mechanism going from NiO to PtO molecules. The relativistic contraction in PtO results in a bond length shorter than that of PdO due to the enhanced covalence of the Pt–O bond.

4. ANALYSIS OF ONiO, OPdO, AND OPtO

ONiO

The 364-nm warm magic angle photoelectron spectrum of $ONiO^-$ is shown in Fig. 6. The spectrum shows relatively few features within 3.408 eV of available photon energy, resulting from the loss of energy analyzer sensitivity for electron kinetic energies less than about 0.2 eV. The other remarkable feature of the spectrum is the substantial, quasi-continuous background throughout the region of photoelectron signals. Such a continuum is generally a result of spectral congestion arising from low–frequency modes with significant frequency change between anion and neutral. Peaks A and C appear to be part of a Franck–Condon progression of peaks, with the much more intense peak (A) being the origin. It is therefore assigned as the electron affinity at 3.043 ± 0.005 eV (see Table 8). Recently, Wu and Wang (*15*) reported the photoelectron spectra of both NiO_2^- and $ONiO^-$. Our result agrees nicely with their measurement of $EA(\mathrm{ONiO}) = 3.05(1)$ eV. Furthermore, Gutsev *et al.* (*40*) calculate an electron affinity of $EA(\mathrm{ONiO}) = 3.25$ eV, consistent with the measurement presented here.

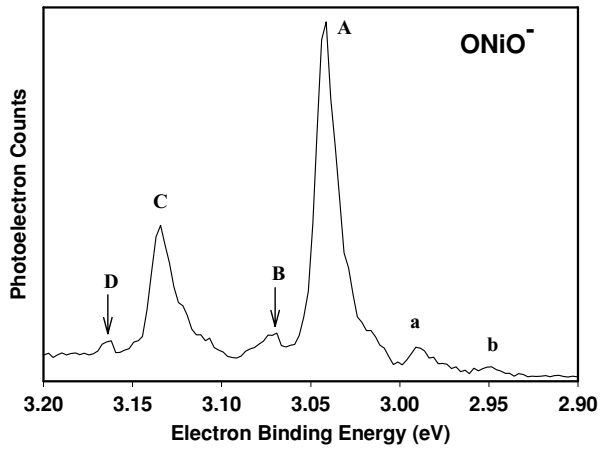

FIG. 6. 364-nm magic angle photoelectron spectrum of $ONiO^-$ at flow tube temperature 300 K.

Peak C is separated from the electron affinity peak by 745(30) cm^{-1}, in good agreement with Wang *et al.* (*15*), who measure a vibrational frequency of 750 cm^{-1}. This peak is the fundamental symmetric stretch vibration of ONiO. Peaks B and D are small features, each located to the higher binding energy side of the $\tilde{X}v = 0$ and 1 peaks by $\approx$250 cm^{-1}. Peaks B and D retain the same relative intensities in the cold sample ONiO photoelectron spectrum (not shown), ruling out vibrational hot bands as a possible assignment. Peaks a and b to the lower binding energy side of peak A vanish upon the cooling of the sample and are assigned as hot bands. The quasicontinuous background also diminishes substantially in the cold spectrum, consistent with the low-frequency hot band supposition above. Peak b is 715 cm^{-1} from peak A, similar to the 750 cm^{-1} stretch in the neutral, and therefore, 715 cm^{-1} is taken to be the anion symmetric stretch frequency. The separation between peak a and peak A, 425(40) cm^{-1}, seems large for an anion bending

TABLE 8
Electron Affinity and Vibrational Frequency Measurements and Literature Values for the OXO $^1\Sigma_g^+ \leftarrow {}^2A_2$ OXO^- (X = Ni, Pd, Pt) Photoelectron Spectra

OXO	*EA* (OXO) (eV)[a]	Literature (eV)	Symmetric Stretch ν (cm^{-1})	Literature (cm^{-1})	r_{X-O} (Å)
$ONiO^-$			715 ± 30		
ONiO	3.043 ± 0.005	3.05 ± 0.01[b]	745 ± 30	750 ± 30[b]	
		3.25[c]		819[c]	
OPdO	3.086 ± 0.005		680 ± 30	730[d]	
$OPtO^-$			760 ± 35	870[f]	r_{Pt-O-}
OPtO	2.677 ± 0.005	2.72 ± 0.20[e]	895 ± 30	980[f]	$r_{Pt-O-} - 0.07(1)$

[a] This work.
[b] Photoelectron spectroscopy: Ref. (*15*).
[c] DFT calculation: Ref. (*40*).
[d] B3LYP calculation: Ref. (*29*).
[e] Thermodynamic cycle determination: Ref. (*39*).
[f] B3LYP calculation, unscaled, this paper.

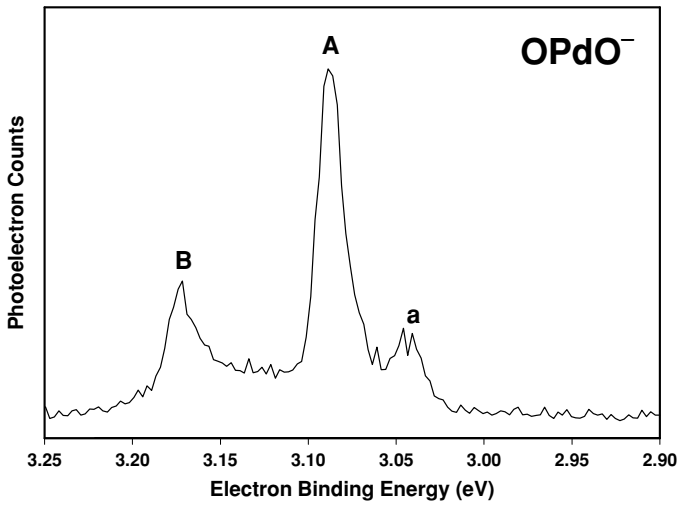

FIG. 7. 364-nm photoelectron spectrum of $OPdO^-$ taken at magic angle polarization and flow tube temperature 200 K.

mode, but might signal a low-lying electronically excited anion state.

It is expected that ONiO has a linear structure (*68*). Gutsev *et al.* (*40*) calculate a linear $^1\Sigma_g^+$ ground state of ONiO with an 819 cm^{-1} symmetric stretch frequency, which confirms our vibrational assignment (see Table 8). They also calculate a slightly bent $^2A_2$ anion ground state with a 170° ONiO bond angle. For both species, the calculated bending frequency is very low (81 cm^{-1} for the neutral and 50 cm^{-1} for the anion), making the molecule very floppy; this result is consistent with the observed congestion and makes the assignment of the 425 cm^{-1} feature as a bending mode very unlikely. It is possible that peaks B and D therefore originate from transitions into two quanta of a neutral low-frequency antisymmetric bending mode, but this assignment would suggest a larger error in the calculated bending frequency (210 cm^{-1} vs 81 cm^{-1}) than appears likely. We note that Gutsev *et al.* (*40*) calculate a low-lying $^3A_2$ ONiO state at excitation energy 560 cm^{-1}. However, there is no obvious reason that photodetachment to produce this triplet state should be as weak as would be the case if peaks B and D arose from transitions to the $^3A_2$ ONiO state. The spectrum of $ONiO^-$ yields a β value of -0.2, essentially an isotropic angular distribution.

OPdO

The 364-nm magic angle cold photoelectron spectrum of $OPdO^-$ is shown in Fig. 7. The spectrum is remarkably similar to that of $ONiO^-$ in Fig. 6, including the significant spectral congestion indicative of significant activity in very-low-frequency vibrational mode(s). Peak A is assigned as the electron affinity at 3.086 ± 0.005 eV. Peak B, 680 cm^{-1} above the electron affinity peak, corresponds to one quantum in the symmetric stretch. There are no experimental data with which to compare these values. Gutsev *et al.* (*40*) find a linear $^1\Sigma_g^+$ ground state for ONiO and this is assumed to be true for OPdO and OPtO (*26, 29*). Bare *et al.* (*29*) obtain a linear OPdO $^1\Sigma_g$ state with 730 cm^{-1} symmetric stretch frequency, which agrees with the value reported here.

Peak a falls 340 cm^{-1} to the lower binding energy side of the electron affinity. This peak retains the same relative intensity in both the warm (not shown) and cold flow tube temperature spectra, thus it is not likely a vibrational hot band. This suggests that peak a from an electronically excited state in the anion.

OPtO

The magic angle, 364-nm cold photoelectron spectrum of $OPtO^-$ is displayed in Fig. 8. It is immediately apparent that this spectrum is qualitatively different from that of either ONiO or OPdO. The electron affinity is substantially lower, the effects of low-frequency vibrational modes are absent, and there are extended vibrational progressions that indicate significant geometry changes upon electron detachment. Peaks a, b, and c exhibit a significant temperature dependence whereas peaks A through E do not. Peak A is assigned as the 0–0 transition from the anion, yielding $EA(OPtO) = 2.677 \pm 0.005$ eV. The photoelectron spectrum of $OPtO^-$ contrasts with those of $ONiO^-$ and $OPdO^-$, in that the lower electron affinity of OPtO (2.7 eV versus 3.1 eV—see Table 8) allows a larger number of accessible features with photon energy 3.408 eV. Our measured *EA* is in agreement with the 2.72 ± 0.20 eV value reported by Rudnyi and co-workers (*39*), although the error is reduced by a factor of 40. Peaks A through E represent transitions into four quanta of a single vibrational mode in the ground electronic state of OPtO, the symmetric stretch with a fundamental frequency of 895 cm^{-1}.

As stated above, peaks a, b, and c are hot bands. From the position of peak a ($v' = 1$) and b ($v' = 2$) with respect to the electron affinity, one vibrational frequency of $OPtO^-$ is obtained, 760 cm^{-1}. However, the spacing between peaks b and c is larger that between a and b by more than 100 cm^{-1}. The width of peak

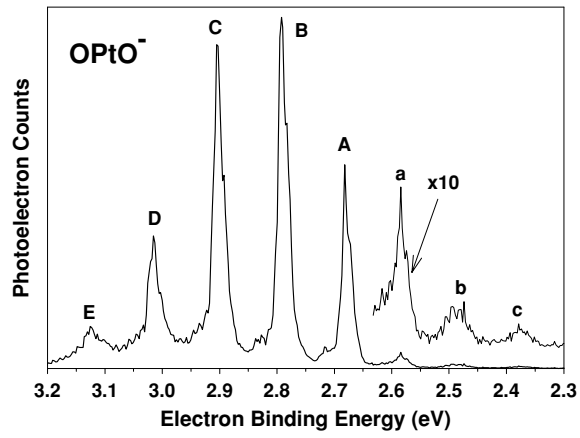

FIG. 8. 364-nm photoelectron spectrum of $OPtO^-$ taken at magic angle polarization and flow tube temperature 200 K.

c suggests that it likely has two contributors: the $v' = 3$ transition from the anion and an electronically excited state of the anion.

Because the OPtO photoelectron spectrum consists of an extended vibrational progression with several resolved peaks, it was simulated using a Franck–Condon empirical fitting routine (*55*). In this way we were able to fit the change in molecular geometry to the spectrum features. Assuming a symmetric linear molecule, the Pt–O bond length changes by 0.07 ± 0.01 Å upon electron detachment. If OPtO behaves as calculated (*40*) for ONiO, then this change would correspond to shortening of the Pt–O bond upon electron detachment. For further details, see Ref. (*49*).

Ab initio frequencies and molecular geometries were also calculated for OPtO and $OPtO^-$. The calculations employed the hybrid density functional theory (DFT) method B3LYP, and the SDD effective core potential/basis set was used for Pt while the aug-cc-pVTZ basis set was used for oxygen, as implemented in the GAUSSIAN 98 suite of programs (*69*). The Pt–O bond length in the anion was found to be 1.778 Å while that of the neutral was shorter at 1.707 Å. This bond contraction of 0.071 Å is in excellent agreement both with the analysis above and with the contraction calculated for ONiO (*40*). Table 8 shows calculated frequency values that agree very well with the experimental values, when scaled by an empirical 0.93 factor. In agreement with previous calculations (*29*), both $OPtO^-$ and OPtO ground states are predicted to be linear.

In contrast to $ONiO^-$, a value of 0.6 was obtained for the anisotropy parameter (β) across the different peaks of the spectra of both $OPtO^-$ and $OPdO^-$. This value is consistent with electron detachment from a molecular orbital of π symmetry and agrees with values obtained for similar systems where a π electron is detached, as in the case of WO_2^- (*70*). The calculations agree with this picture, indicating that the extra electron in the anion is occupying a π^* molecular orbital. This result also agrees with the fact that the anion shows a smaller stretching frequency that the neutral, suggesting that the extra electron in the anion is occupying an antibonding orbital.

5. CONCLUSIONS

The 364-nm photoelectron spectra of XO^- and OXO^- anions (X = Ni, Pd, and Pt) were recorded and analyzed. Electron affinities ($^3\Sigma^- \leftarrow {}^2\Pi_{3/2}$)were identified for all three XO^- spectra. Anion $^2\Pi_{3/2}$–$^2\Pi_{3/2}$ spin–orbit splittings were identified as well as neutral $^3\Pi_2$–$^3\Pi_1$ spin–orbit splittings for NiO, PdO, and PtO. Several of the assignments for NiO and PdO were corrected from existing literature values. Some vibrational activity was observed in the spectra of NiO^-, none in PdO^-, and significantly more was observed in PtO^-, with larger bond length changes measured than in the spectra of NiO^-. The majority of electronic transitions observed in the NiO^- spectrum and all transitions in the PdO^- spectrum occurred by detaching nonbonding electrons, whereas in PtO^- the detached electrons had more antibonding quality. This observation, in addition to molecular spin–orbit splitting values, attests to the large covalent character of the PtO bond with respect to the NiO and PdO bonds. Electron affinities and symmetric stretch vibrational frequencies were extracted from the spectra of the OXO^- molecules, as well as an O–X bond length change in OPtO.

ACKNOWLEDGEMENTS

The authors thank the National Science Foundation and the Air Force Office of Scientific Research for support of this work. The Swedish Foundation for International Cooperation in Research and Higher Education (STINT) has also provided valuable financial assistance.

REFERENCES

1. H. Y. H. Chan, S. Zou, and M. J. Weaver, *J. Phys. Chem. B* **103,** 11 141–11 151 (1999).
2. T. Sasaki, N. Koshizaki, and K. M. Beck, *Appl. Phys. A Mater. Sci. Process.* **69,** S771–S774 (1999).
3. L. Maya, L. Riester, T. Thundat, and C. S. Yust, *J. Appl. Phys.* **84,** 6382–6386 (1998).
4. O. L. Shcheka, N. V. Dobrodey, and T. B. Emelina, *Int. J. Quantum Chem.* **50,** 181–188 (1994).
5. G. Boschloo and A. Hagfeldt, *J. Phys. Chem. B* **105,** 3039–3044 (2001).
6. S. C. Su, J. N. Carstens, and A. T. Bell, *J. Catal.* **176,** 125–135 (1998).
7. V. Biju and M. Abdul Khadar, *J. Mater. Sci.* **36,** 5779–5787 (2001).
8. J. R. Mc Bride, G. W. Graham, C. R. Peters, and W. H. Weber, *J. Appl. Phys.* **69,** 1596–1604 (1991).
9. D. W. Green, G. T. Reedy, and J. G. Kay, *J. Mol. Spectrosc.* **78,** 257–266 (1979).
10. V. I. Srdanov and D. O. Harris, *J. Chem. Phys.* **89,** 2748–2753 (1988).
11. E. J. Friedman-Hill and R. W. Field, *J. Mol. Spectrosc.* **155,** 259–276 (1992).
12. R. S. Ram and P. F. Bernath, *J. Mol. Spectrosc.* **155,** 315–325 (1992).
13. K.-I. Namiki and S. Saito, *Chem. Phys. Lett.* **252,** 343–347 (1996).
14. A. Citra, G. V. Chertihin, L. Andrews, and M. Neurock, *J. Phys. Chem. A* **101,** 3109–3118 (1997).
15. H. Wu and L.-S. Wang, *J. Chem. Phys.* **107,** 16–21 (1997).
16. V. D. Moravec and C. C. Jarrold, *J. Chem. Phys.* **108,** 1804–1810 (1998).
17. C. W. Bauschlicher, Jr., C. J. Nelin, and P. S. Bagus, *J. Chem. Phys.* **82,** 3265–3276 (1985).
18. C. W. Bauschlicher, Jr., *Chem. Phys.* **93,** 399–404 (1985).
19. S. P. Walch and W. A. Goddard, *J. Am. Chem. Soc.* **100,** 1338–1348 (1978).
20. M. Dolg, U. Wedig, H. Stoll, and H. Preuss, *J. Chem. Phys.* **86,** 2123–2131 (1987).
21. E. G. Bakalbassis, M.-A. D. Stiakaki, A. C. Tsipis, and C. A. Tsipis, *Chem. Phys.* **205,** 389–399 (1996).
22. E. Lorda, F. Illas, and P. S. Bagus, *Chem. Phys. Lett.* **256,** 377–382 (1996).
23. A. J. Bridgeman, *J. Chem. Soc. Dalton. Trans.*, 4555–4562 (1996).
24. P. Schwerdtfeger, J. S. Mcfeaters, J. J. Moore, D. M. Mcpherson, R. P. Cooney, G. A. Bowmaker, M. Dolg, and D. Andrae, *Langmuir* **7,** 116–125 (1991).
25. P. E. M. Siegbahn, *Chem. Phys. Lett.* **201,** 15–23 (1993).
26. P. E. M. Siegbahn, *J. Phys. Chem.* **97,** 9096–9102 (1993).
27. S.-C. Chung, S. Kruger, G. Pacchioni, and N. Rosch, *J. Chem. Phys.* **102,** 3695–3702 (1995).
28. E. Broclawik, R. Yamauchi, A. Endou, M. Kubo, and A. Miyamoto, *J. Chem. Phys.* **104,** 4098–4104 (1996).
29. W. D. Bare, A. Citra, G. V. Chertihin, and L. Andrews, *J. Phys. Chem. A* **103,** 5456–5462 (1999).
30. A. Dedieu, *Chem. Rev.* **100,** 543–600 (2000).
31. S. A. Klopcic, V. D. Moravec, and C. C. Jarrold, *J. Chem. Phys.* **110,** 10 216–10 217 (1999).

32. C. Nilsson, R. Scullman, and N. Mehendale, *J. Mol. Spectrosc.* **35,** 172–189 (1970).
33. R. Scullman, U. Sassenberg, and C. Nilsson, *Can. J. Phys.* **53,** 1991–1999 (1975).
34. K. Jansson and R. Scullman, *J. Mol. Spectrosc.* **61,** 299–312 (1976).
35. U. Sassenberg and R. Scullman, *J. Mol. Spectrosc.* **68,** 331–332 (1977).
36. U. Sassenberg and R. Scullman, *Phys. Scr.* **28,** 139–149 (1983).
37. C. I. Frum, R. Engleman, Jr., and P. F. Bernath, *J. Mol. Spectrosc.* **150,** 566–575 (1991).
38. E. J. J. Kirchner, E. J. Baerends, U. Van Slooten, and A. W. Kleyn, *J. Chem. Phys.* **97,** 3821–3830 (1992).
39. E. B. Rudnyi, O. V. Kuznetsova, E. A. Kaibicheva, and L. N. Sidorov, *Temperatur* **28,** 864–870 (1991).
40. G. L. Gutsev, B. K. Rao, and P. Jena, *J. Phys. Chem. A* **104,** 11 961–11 971 (2000).
41. M. L. Polak, M. K. Gilles, J. Ho, and W. C. Lineberger, *J. Phys. Chem.* **95,** 3460–3462 (1991).
42. H. Wu, S. R. Desai, and L.-S. Wang, *J. Phys. Chem. A* **101,** 2103–2111 (1997).
43. X. Li and L.-S. Wang, *J. Chem. Phys.* **109,** 5264–5268 (1998).
44. V. D. Moravec and C. C. Jarrold, *J. Chem. Phys.* **112,** 792–798 (2000).
45. S. A. Klopcic, V. D. Moravec, and C. C. Jarrold, *J. Chem. Phys.* **110,** 8986–8991 (1999).
46. A. J. Merer, *Annu. Rev. Phys. Chem.* **40,** 407–38 (1989).
47. P. Pyykko, *Chem. Rev.* **88,** 563–594 (1988).
48. K. M. Ervin and W. C. Lineberger, *in* "Advances in Gas Phase Ian Chemistry" (N. G. Adams and L. M. Babcock, Eds.), Vol. 1, pp. 121–166. JAI Press, Greenwich, 1992.
49. T. M. Ramond, Ph.D. dissertation, University of Colorado, 2001.
50. J. Ho, Ph.D. dissertation, University of Colorado, 1991.
51. J. Ho, K. M. Ervin, and W. C. Lineberger, *J. Chem. Phys.* **93,** 6987–7002 (1990).
52. D. M. Neumark, K. R. Lykke, T. Andersen, and W. C. Lineberger, *Phys. Rev. A* **32,** 1890–1892 (1985).
53. C. E. Moore, "Atomic Energy Levels," US GPO Circular No. 467. Washington, DC, 1952.
54. J. Cooper and R. N. Zare, *J. Chem. Phys.* **48,** 942 (1968).
55. K. M. Ervin, *PESCAL99*. 1999.
56. C. W. Bauschlicher, Jr. and P. Maitre, *Theor. Chim. Acta* **90,** 189–203 (1995).
57. J. Ho, M. L. Polak, and W. C. Lineberger, *J. Chem. Phys.* **96,** 144–154 (1992).
58. C. C. Arnold, C. S. Xu, G. R. Burton, and D. M. Neumark, *J. Chem. Phys.* **102,** 6982–6989 (1995).
59. T. N. Kitsopoulos, C. J. Chick, Y. Zhao, and D. M. Neumark, *J. Chem. Phys.* **95,** 1441–1448 (1991).
60. V. D. Moravec, S. A. Klopcic, and C. C. Jarrold, *J. Chem. Phys.* **110,** 5079–5088 (1999).
61. J. Ho, M. L. Polak, and W. C. Lineberger, *J. Chem. Phys.* **96,** 144–54 (1992).
62. C. W. Bauschlicher, Jr., S. R. Langhoff, H. Partridge, and M. Sodupe, *J. Phys. Chem.* **97,** 856–859 (1993).
63. M. Scheer, C. A. Brodie, R. C. Bilodeau, and H. K. Haugen, *Phys. Rev. A* **58,** 2051–2062 (1998).
64. T. C. Steimle, K. Y. Jung, and B.-Z. Li, *J. Chem. Phys.* **103,** 1767–1772 (1995).
65. L. C. O' Brien, S. J. Wall, and M. K. Sieber, *J. Mol. Spectrosc.* **183,** 57–60 (1997).
66. P. F. Bernath, "Spectra of Atoms and Molecules." Oxford Univ. Press, New York, 1995.
67. J. Thogersen, M. Scheer, L. D. Steele, and H. K. Haugen, *Phys. Rev. Lett.* **76,** 2870–2873 (1996).
68. R. J. Van Zee, Y. M. Hamrick, S. Li, and W. Weltner, Jr., *J. Phys. Chem.* **96,** 7247–7251 (1992).
69. M. J. Frisch, G. W. Trucks, H. B. Schlegel, G. E. Scuseria, M. A. Robb, J. R. Cheeseman, V. G. Zakrzewski, J. A. Montgomery, R. E. Stratmann, J. C. Burant, S. Dapprich, J. M. Millam, A. D. Daniels, K. N. Kudin, M. C. Strain, O. Farkas, J. Tomasi, V. Barone, M. Cossi, R. Cammi, B. Mennucci, C. Pomelli, C. Adamo, S. Clifford, J. Ochterski, G. A. Petersson, P. Y. Ayala, Q. Cui, K. Morokuma, D. K. Malick, A. D. Rabuck, K. Raghavachari, J. V. Foresman, J. Cioslowski, J. V. Ortiz, A. G. Baboul, B. B. Stefanov, G. Liu, A. Liashenko, P. Piskorz, I. Komaromi, R. Gomperts, R. L. Martin, D. J. Fox, T. Keith, M. A. Al-Laham, C. Y. Peng, A. Nanayakkara, C. Gonzales, M. Challacombe, P. M. W. Gill, B. Johnson, W. Chen, M. W. Wong, J. L. Andres, M. Head-Gordon, E. S. Replogle, and J. A. Pople, Gaussian 98. Gaussian, Inc., 1998.
70. G. E. Davico, R. L. Schwartz, T. M. Ramond, and W. C. Lineberger, *J. Phys. Chem. A* **103,** 6167–6172 (1999).